Check for updates

JAMES | Journal of Advances in Modeling Earth Systems

RESEARCH ARTICLE
10.1029/2022MS003516

Special Section:
Using radiative-convective equilibrium to understand convective organization, clouds, and tropical climate

Effects of Circulation on Tropical Cloud Feedbacks in High-Resolution Simulations

Anna Mackie[1] and **Michael P. Byrne**[1,2]

[1]School of Earth and Environmental Sciences, University of St Andrews, St Andrews, UK, [2]Atmospheric, Oceanic and Planetary Physics, University of Oxford, Oxford, UK

Abstract Uncertainty in the response of clouds to global warming remains a significant barrier to reducing uncertainty in climate sensitivity. A key question is the extent to which the dynamic component—that which is due to changes in circulation rather than changes in the thermodynamic properties of clouds—contributes to the total cloud feedback. Here, simulations with a range of cloud-resolving models are analyzed to quantify the impact of circulation changes on tropical cloud feedbacks. The dynamic component of the cloud feedback is substantial for some models and is controlled both by sea surface temperature (SST) induced changes in circulation and nonlinearity in the climatological relationship between clouds and circulation. We find notable inter-model differences in the extent to which ascending regions narrow or expand in response to a change in SST, which we link to differences in the longwave and shortwave dynamic components across models. The diversity of changes in ascent area is coupled to intermodel differences in non-radiative diabatic heating in ascending regions.

Plain Language Summary Clouds influence Earth's energy balance by absorbing and reflecting solar and terrestrial radiation. The response of clouds to warming remains a key source of uncertainty in understanding how the climate system will evolve. In particular, how the influence of clouds on radiation is coupled to the atmospheric circulation is an open question. In this study, idealized simulations of the tropics at high spatial resolution (3 km) are analyzed to probe how changes in circulation impact clouds in a warming climate. It is found that, across a range of models, the degree to which circulation changes influence clouds depends on how the area of the region with ascending air responds to warming.

Key Points:

- Influence of circulation changes on cloud feedbacks is substantial in some cloud-resolving models
- Component of cloud feedback associated with circulation changes is coupled to ascent area
- Intermodel spread in response of ascent area linked to non-radiative diabatic heating

Supporting Information:

Supporting Information may be found in the online version of this article.

Correspondence to:

A. Mackie,
arm33@st-andrews.ac.uk

Citation:

Mackie, A., & Byrne, M. P. (2023). Effects of circulation on tropical cloud feedbacks in high-resolution simulations. *Journal of Advances in Modeling Earth Systems*, *15*, e2022MS003516. https://doi.org/10.1029/2022MS003516

Received 9 NOV 2022
Accepted 22 APR 2023

© 2023 The Authors. Journal of Advances in Modeling Earth Systems published by Wiley Periodicals LLC on behalf of American Geophysical Union. This is an open access article under the terms of the Creative Commons Attribution License, which permits use, distribution and reproduction in any medium, provided the original work is properly cited.

1. Introduction

The interplay between clouds and the atmospheric circulation is a persistent source of uncertainty in our understanding of how the climate system will evolve (Bony et al., 2015; Ceppi et al., 2017; Sherwood et al., 2014; Webb et al., 2017). One particular challenge is that clouds and their associated radiative effects—particularly in the tropics—are strongly influenced by convection (Hartmann et al., 2001), which occurs at horizontal scales smaller than those typically resolved by the current generation of global climate models (GCMs). Integrating GCMs at convection-permitting resolutions for long enough to study climate and climate change remains prohibitively expensive. One way to overcome this computational barrier is through the use of limited-domain cloud-resolving models (CRMs), which have the potential to advance fundamental understanding of cloud–circulation coupling in the tropics and shed light on potential sources of uncertainty in cloud feedbacks.

Cloud radiative effect—defined as the difference between all-sky and clear-sky broadband fluxes at the top-of-atmosphere (TOA), with positive values representing a net downward flux at TOA due to clouds—is tightly coupled to the atmospheric circulation (Bony et al., 2004). In the tropics, regions of strong ascent are associated with strong positive longwave cloud radiative effects due to their high, cold cloud tops and therefore large temperature contrast relative to the surface. These deep convective clouds are also highly reflective, resulting in co-located regions of strong negative shortwave cloud radiative effect (Hartmann et al., 2001; Kiehl, 1994). There is a clear correspondence between areas of ascent and descent, as measured by vertical velocity in the mid-troposphere (500 hPa), and longwave and shortwave cloud radiative effect (Figures 1 and 2). As the change in cloud radiative effect with temperature also includes masking effects (e.g., Soden et al., 2008), for example, due to water vapor, it does not isolate the feedback due solely to clouds. Here, for simplicity, we approximate the cloud feedback as the change in cloud radiative effect divided by the sea surface temperature (SST) change (e.g.,

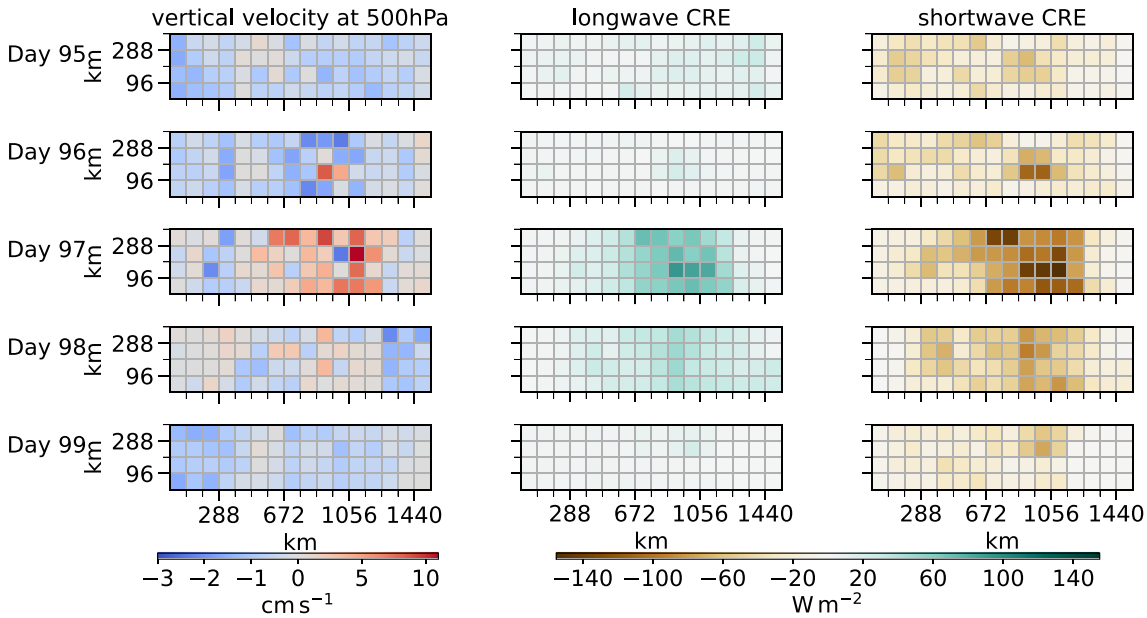

Figure 1. Daily-mean snapshots of vertical velocity at 500 hPa (left), longwave cloud radiative effect (LW CRE, middle) and shortwave cloud radiative effect (SW CRE, right) from a simulation with uniform sea surface temperature (300 K) performed by the SAM_CRM model (Table A1). Data have been spatially (96 × 96 km blocks) and temporally averaged (24-hr periods). Positive values of cloud radiative effect correspond to a warming effect of clouds at TOA. Note the different positive and negative color scales for vertical velocity (left).

Bony & Dufresne, 2005). Future work could adjust the changes in cloud radiative effect to account for masking effects, for example, using the technique of Cronin and Wing (2017).

There are a number of ways in which tropical convective-scale circulations may change in a warming climate. For example, previous work with CRMs has suggested that a warmer climate may lead to stronger updraft velocities (Singh & O'Gorman, 2015); more convective available potential energy (Romps & Kuang, 2011); changes to convective organization (Wing & Emanuel, 2014); a weakening of the overturning circulation and changes to the area of ascending air (Cronin & Wing, 2017; Jenney et al., 2020). However, it remains unclear to what extent these circulation changes could impact cloud feedbacks.

The dependence of clouds on circulation is often characterized by discretizing cloud radiative effect as a function of circulation regime, with regimes typically defined in terms of the mid-tropospheric vertical velocity (Bony et al., 2004; Bony et al., 2006; Byrne & Schneider, 2018; Lutsko, 2018; Wyant, Bretherton, et al., 2006) (Figures 2a and 2b). Previous work has shown that there exists an approximately linear relationship between cloud radiative effect and vertical velocity in GCMs with $\mathcal{O}(1°)$ horizontal resolution for a broad range of circulation regimes (Byrne & Schneider, 2018), and that this quasi-linearity constrains the influence of circulation changes on cloud feedbacks to be small (Byrne & Schneider, 2018; Wyant, Bretherton, et al., 2006). But as $\mathcal{O}(1°)$-resolution GCMs cannot resolve the convective-scale circulations that influence cloud radiative effect, particularly in tropical and subtropical regions, this raises the following questions: Is the impact of circulation changes on cloud feedbacks small when convection is explicitly simulated? Or do circulation changes and their impacts on cloud feedbacks become more dominant at higher resolutions, representing a potentially important influence on cloud feedbacks that is absent from the current generation of GCMs?

This study will address three questions: First, do the climatological relationships between circulation and cloud radiative effect in CRMs display the same quasi-linearity as found in GCMs? Second, in CRMs, are the dynamic components of cloud feedbacks—due to changes in circulation—a significant part of the total feedback? And third, which physical processes control the dynamic components across a range of CRMs? We begin with an overview of the models and simulations to be analyzed (Section 2), followed by a description of how cloud feedbacks are decomposed into dynamic and thermodynamic components (Section 3). We then develop, in Section 3.1, a toy model to explore the effects of nonlinearities in climatological cloud-circulation coupling on cloud feedbacks. In Sections 4 and 5 we analyze the physical processes controlling the dynamic components across CRMs, before concluding with a discussion and suggestions for future research (Section 6).

19422466, 2023, 5, Downloaded from https://agupubs.onlinelibrary.wiley.com/doi/10.1029/2022MS003516 by University Of St Andrews University, Wiley Online Library on [15/05/2023]. See the Terms and Conditions (https://onlinelibrary.wiley.com/terms-and-conditions) on Wiley Online Library for rules of use; OA articles are governed by the applicable Creative Commons License

19422466, 2023, 5, Downloaded from https://agupubs.onlinelibrary.wiley.com/doi/10.1029/2022MS003516 by University Of St Andrews University, Wiley Online Library on [15/05/2023]. See the Terms and Conditions (https://onlinelibrary.wiley.com/terms-and-conditions) on Wiley Online Library for rules of use; OA articles are governed by the applicable Creative Commons License

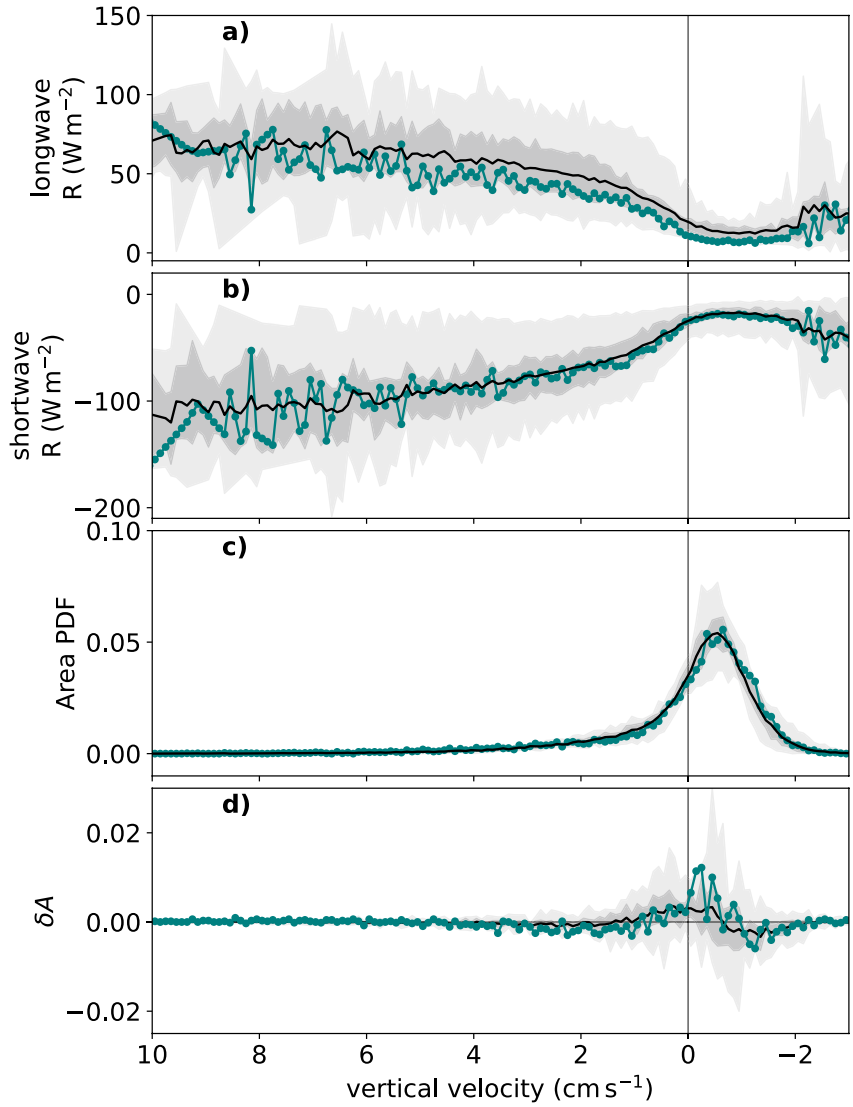

Figure 2. Panel (a) Longwave cloud radiative effect; panel (b) shortwave cloud radiative effect; and panel (c) area probability density function, all expressed as functions of vertical velocity at 500 hPa for the 295 K simulations. Panel (d): Change in area PDFs between the 295 and 300 K simulations. Light gray shading indicates the full range of RCEMIP models, dark gray shading the interquartile range, and the black continuous lines show the multimodel means. Data from SAM_CRM is in turquoise. Note that the *x*-axis has been truncated in order to focus on the most populated vertical velocity bins: the full range of vertical velocity is 21.95–−6.95 cm s^{-1}.

2. Simulations

A common framework to study cloud-circulation interactions is radiative-convective equilibrium (RCE), an idealization of the tropical atmosphere defined by a simple thermodynamic balance between radiative cooling and convective heating (e.g., Held et al., 1993). The major advantage of RCE is its conceptual simplicity, which permits fundamental convective and cloud processes to be studied without additional complicating effects such as rotation or equator-to-pole temperature gradients (Wing et al., 2020). RCE can be implemented across spatial scales and used to study various aspects of the tropical atmosphere: For example, previous studies have focused on the factors controlling cloud anvil amount in GCMs and CRMs (Bony et al., 2016); the relationship between organization of convection and extreme precipitation (Bao et al., 2017; Pendergrass et al., 2016); energetic constraints on large-scale circulations (Jenney et al., 2020); the response of updraft velocities to warming (Singh & O'Gorman, 2015); and self aggregation of convection (Bretherton et al., 2005; Holloway & Woolnough, 2016;

19422466, 2023, 5, Downloaded from https://agupubs.onlinelibrary.wiley.com/doi/10.1029/2022MS003516 by University Of St Andrews University, Wiley Online Library on [15/05/2023]. See the Terms and Conditions (https://onlinelibrary.wiley.com/terms-and-conditions) on Wiley Online Library for rules of use; OA articles are governed by the applicable Creative Commons License

Muller & Held, 2012; Wing & Emanuel, 2014). In this study we will primarily use CRMs to assess the degree to which circulation influences cloud feedbacks in simulations of RCE.

A recent model intercomparison project (the Radiative-Convective Equilibrium Intercomparison Project, RCEMIP) has established an archive of CRM and GCM simulations of RCE over a range of resolutions and SSTs (Wing et al., 2018, 2020). Despite uniform boundary conditions, there are substantial differences in simulated states across the RCEMIP models, with large differences in temperature, relative humidity and cloud profiles (Wing et al., 2020). Cloud and circulation responses to warming also vary across the models (Becker & Wing, 2020; Silvers et al., 2023), though the majority simulate anvil clouds which rise, warm and reduce in area fraction with SST warming, consistent with previous work (Bony et al., 2016; Hartmann & Larson, 2002; Zelinka & Hartmann, 2010). The RCEMIP models also have a large spread in their "Cess-type" TOA feedback parameters (Cess & Potter, 1988)—defined as the change in net TOA radiation divided by the surface temperature change—leading to a spread in their hypothetical climate sensitivities (Becker & Wing, 2020; Wing et al., 2020). In particular, Becker and Wing (2020) determine that model differences in the total feedback parameter and climate sensitivity arise through a combination of the differing temperature dependencies of shallow cloud fraction and convective aggregation across models.

A major advantage of RCEMIP is that it incorporates a hierarchy of models run in RCE, with consistent experiments allowing comparison across model types. Here, we focus on the simulations at 3 km resolution in a long-channel domain (~6,000 km × ~400 km) which explicitly simulate convection. These long-channel simulations permit both convection and the evolution of large-scale dynamics within the domain (Cronin & Wing, 2017; Wing & Cronin, 2016). All models used are listed in Table Appendix A. Detailed information about individual models can be found in the Supporting Information of Wing et al. (2020). All simulations are non rotating, with uniform solar insolation and uniform, fixed SST at three different temperatures (295, 300, and 305 K).

3. Dynamic and Thermodynamic Components of Cloud Feedbacks

To assess how circulation changes influence cloud feedbacks we follow the framework introduced by Bony et al. (2004) and employed by a number of subsequent studies (Byrne & Schneider, 2018; Lutsko, 2018; Wyant, Bretherton, et al., 2006; Wyant, Khairoutdinov, & Bretherton, 2006), in which changes in the cloud radiative effect at TOA are decomposed into components associated with (a) changes in circulation (the dynamic component) and (b) changes assuming fixed circulation (the thermodynamic component). An additional nonlinear component quantifies the combined influence of changes in circulation and thermodynamic processes on the cloud feedbacks.

We analyze the last 25 days of each simulation, following Wing et al. (2020). For the CRMs, we perform spatial and temporal averaging: We calculate daily means with a spatial average over 96 × 96 km, a similar scale to typical GCM gridboxes which have a resolution on the order of 1–2°. This allows us to investigate cloud–circulation coupling at a spatial scale that is comparable to previous studies using global models (Bony et al., 2004; Byrne & Schneider, 2018), and also improves the computational efficiency of our analysis. We test the sensitivity of key parts of our analysis to this spatial and temporal averaging (Figures S1–S4 in Supporting Information S1, see below for more detail).

To decompose the total cloud feedback into dynamic and thermodynamic components, we first characterize how the cloud radiative effect, in both the longwave and shortwave, depends on vertical velocity at 500 hPa (w). We extract the vertical velocity at the model level closest to 500 hPa for each time- and space-averaged block, then discretize the vertical velocity field into bins of width 0.1 cms^{-1}. This allows us to construct two discretized functions of the longwave and shortwave cloud radiative effects, $R_{LW}(w)$ and $R_{SW}(w)$, which we term the "cloud-circulation coupling functions." Figures 1 and 2 illustrate this process: for all the grid points falling within a particular vertical velocity bin (Figure 1, left column), we calculate the mean of the longwave and shortwave cloud radiative effects (Figure 1, middle and right columns) obtaining $R_{LW}(w)$ and $R_{SW}(w)$ (Figures 2a and 2b). The area probability density function $[A(w)]$ is simply the normalized number of points within each vertical velocity bin (Figure 2c). To construct a continuous function, we linearly interpolate across any empty vertical velocity bins and ensure $A(w)$ integrates to 1 over the full w range by normalizing to account for the linear interpolation.

Figures 2a–2c show the $R_{LW}(w)$, $R_{SW}(w)$, and $A(w)$ functions from the SAM_CRM model in turquoise. Also included are the multimodel mean, interquartile range and full range of the CRMs. Despite the large intermodel

19422466, 2023, 5, Downloaded from https://agupubs.onlinelibrary.wiley.com/doi/10.1029/2022MS003516 by University Of St Andrews University, Wiley Online Library on [15/05/2023]. See the Terms and Conditions (https://onlinelibrary.wiley.com/terms-and-conditions) on Wiley Online Library for rules of use; OA articles are governed by the applicable Creative Commons License

spread, there are some common features across models: While there are relatively few grid points with strong ascent (strongly positive vertical velocity), these regions have large longwave and shortwave cloud radiative effects associated with deep convective clouds. These high-topped clouds are both cold, reducing the outgoing longwave radiation with respect to clear-sky conditions and producing a strong positive longwave cloud radiative effect, and reflective, increasing the proportion of shortwave radiation reflected to space and producing a strong negative shortwave cloud radiative effect. With weakening ascent, we generally see a decrease in the magnitudes of the longwave and shortwave cloud radiative effects (Figures 2a and 2b). The functions $R_{LW}(w)$ and $A(w)$ are broadly similar if constructed by averaging over smaller spatial scales (Figure S1 in Supporting Information S1) and shorter time scales (Figure S2 in Supporting Information S1).

In continuous form, the mean cloud radiative effect can be written as:

$$\overline{R} = \int_{-\infty}^{\infty} R(w)A(w)\mathrm{d}w. \tag{1}$$

The mean change in cloud radiative effect with warming, $\overline{\delta R}$, can then be decomposed into dynamic, thermodynamic and nonlinear components as follows:

$$\overline{\delta R} = \underbrace{\int_{-\infty}^{\infty} R(w)\delta A(w)\mathrm{d}w}_{\text{dynamic}} + \underbrace{\int_{-\infty}^{\infty} \delta R(w)A(w)\mathrm{d}w}_{\text{thermodynamic}} + \underbrace{\int_{-\infty}^{\infty} \delta R(w)\delta A(w)\mathrm{d}w}_{\text{nonlinear}}. \tag{2}$$

The first term on the right hand side of Equation 2 is the dynamic component representing the effect of circulation changes between simulations, $\delta A(w)$, on cloud radiative effect assuming constant cloud–circulation coupling functions (i.e., $\delta R_{LW}(w) = 0$, $\delta R_{SW}(w) = 0$). The second term is the thermodynamic component, which quantifies the change in cloud radiative effect assuming a fixed distribution of vertical velocity (i.e., $\delta A(w) = 0$). The third term is the nonlinear component, which depends on changes in both circulation and cloud–circulation coupling. In physical terms, the dynamic component represents the change in cloud radiative effect due to, say, a strengthening or weakening of vertical velocity in ascending/descending regions, or a change in the relative sizes of these regions, while the thermodynamic component includes, for example, the effects on the cloud radiative effect of phase changes in cloud water. For discussion of these and further examples we refer the reader to Byrne and Schneider (2018).

3.1. Influence of Nonlinearity in Cloud–Circulation Coupling on the Dynamic Component

As illustrated in Figure 2, sections of the cloud–circulation coupling functions $R_{LW}(w)$ and $R_{SW}(w)$ are approximately linear, though the sections where vertical velocities are close to zero deviate substantially from this quasi-linearity, a feature also found in observational data (Bony et al., 2004; Wyant, Bretherton, et al., 2006) and GCMs (Byrne & Schneider, 2018). This quasi-linearity constrains the global dynamic component of the cloud feedback to be small in GCMs: Byrne and Schneider (2018) show that for the theoretical case of a strictly linear cloud–circulation coupling function over a closed-mass region, the dynamic component is zero, regardless of changes in circulation. But in the more general and realistic case where cloud–circulation coupling functions are nonlinear, the dynamic component will depend on higher-order terms in w in the cloud–circulation coupling function ($R(w)$). Here, using a toy model, we explore how different characteristics of the nonlinearity in cloud–circulation coupling control the degree to which circulation changes influence the cloud feedback.

As we are interested in possible reasons for intermodel differences in the magnitude of the dynamic component, shown in Byrne and Schneider (2018) to be dependent on the shape of the cloud–circulation function, we now extend this theoretical analysis. We demonstrate that not only is a nonlinear cloud–circulation coupling function required for a nonzero dynamic component, but that the magnitude of the dynamic component depends on both the degree of nonlinearity in $R(w)$ and its location, in w space, relative to the change in circulation, $\delta A(w)$. To illustrate the sensitivities of the dynamic component to the climatological structure of cloud–circulation coupling, we construct a toy model of $R(w)$:

$$R_{toy}(w) = a + bw + c\tanh(dw + e), \tag{3}$$

where a, b, c, d, and e are constants, with baseline values of $a = 17$, $b = 592$, $c = 32$, $d = 1$ and $e = 0$. The functional form of Equation 3 and values of the constants are chosen so as to qualitatively match a simulated longwave cloud–circulation coupling function (cf. Figures 3a and 3b). By varying the constants c and e we explore,

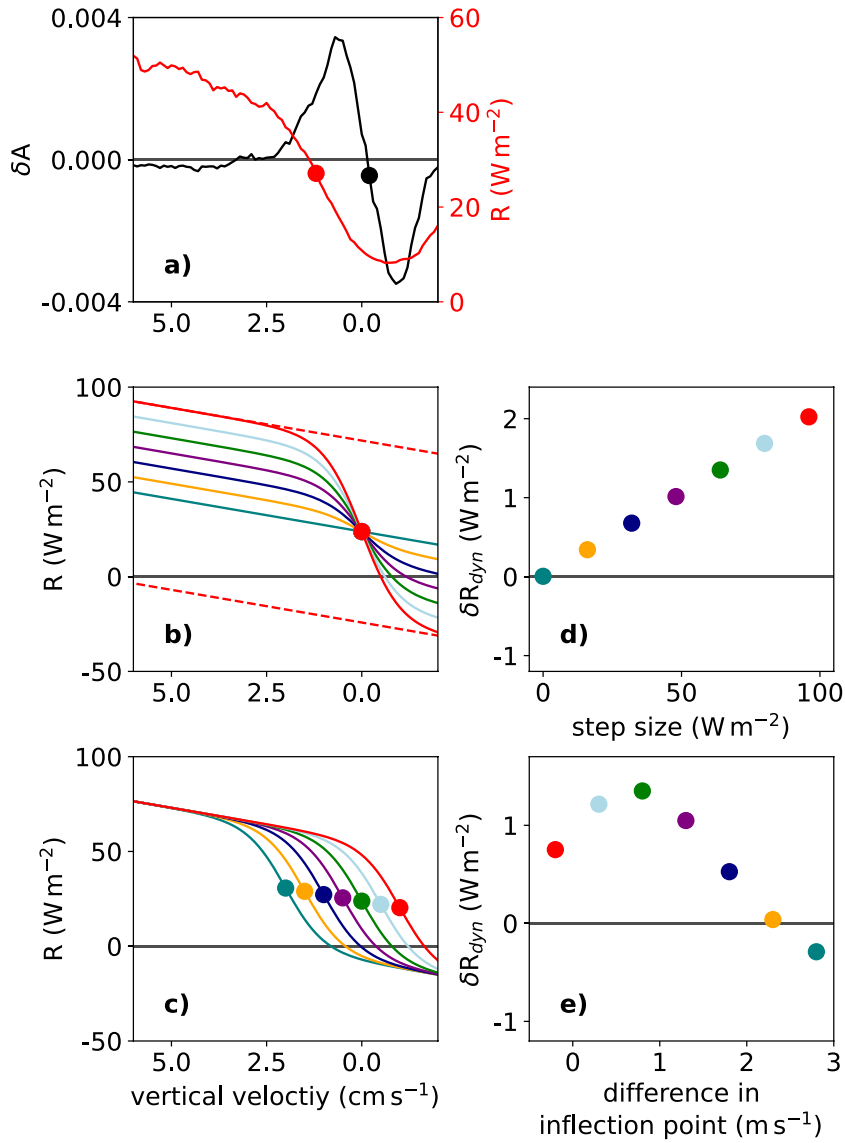

Figure 3. Investigating the effects of nonlinearity in cloud–circulation coupling using a toy model of $R(w)$. Panel (a): Simulated $R(w)$ taken from the SAM_CRM RCE_large300 run, while δA is calculated from SAM_CRM RCE_large305 minus SAM_CRM RCE_large300. Both $R(w)$ and δA are smoothed using a 14-bin moving average over w. Circles indicate the positions of the inflection point in the curves. Panels (b, c): Idealized forms of $R(w)$ generated using Equation 3 by varying the (b) step size and (c) point of inflection. Circles in panels (b, c) indicate the locations of the inflection points in the $R(w)$ functions. Panels (d, e): The dynamic components obtained by multiplying the idealized forms of $R(w)$ from panels (b and c), respectively, with the simulated δA from panel (a) and integrating over w. These are plotted as a function of (d) step size (defined as the difference, in Wm^{-2}, between the two linear extrapolations before and after the nonlinearity: these extrapolations are shown in panel (b) for the case of $c = 48$ as dashed red lines) and (e) the difference in inflection points between $\delta A(w)$ and $R(w)$ (defined, in units of ms^{-1}, as the position of the inflection point in $R(w)$ minus the position of the inflection point in $\delta A(w)$).

respectively, the impacts on the dynamic component of (a) varying the degree of nonlinearity in $R(w)$ and (b) varying the location of the nonlinearity relative to $\delta A(w)$ in w space. The stylized version of $R(w)$ described by Equation 3 is multiplied by the simulated circulation change $\delta A(w)$ from the SAM_CRM model and summed over all vertical velocities to explore, in a general way, how climatological cloud–circulation coupling affects the cloud feedback.

Varying the constant c modulates the difference between two linear extrapolations before and after the nonlinearity in the function. We term this difference, which has units of Wm^{-2}, "step size." As anticipated from the

19422466, 2023, 5, Downloaded from https://agupubs.onlinelibrary.wiley.com/doi/10.1029/2022MS003516 by University Of St Andrews University, Wiley Online Library on [15/05/2023]. See the Terms and Conditions (https://onlinelibrary.wiley.com/terms-and-conditions) on Wiley Online Library for rules of use; OA articles are governed by the applicable Creative Commons License

19422466, 2023, 5, Downloaded from https://agupubs.onlinelibrary.wiley.com/doi/10.1029/2022MS003516 by University Of St Andrews University, Wiley Online Library on [15/05/2023]. See the Terms and Conditions (https://onlinelibrary.wiley.com/terms-and-conditions) on Wiley Online Library for rules of use; OA articles are governed by the applicable Creative Commons License

discussion above and following the results of Byrne and Schneider (2018), when $R(w)$ is linear ($c = 0$, turquoise line in Figure 3b), the resultant dynamic component is identically zero (turquoise circle in Figure 3d). As the nonlinearity is enhanced by increasing c, the magnitude of the dynamic component increases (Figure 3d). Thus, Figure 3d shows that the magnitude of the dynamic effect increases approximately linearly with step size.

Varying the location of the nonlinearity in the cloud–circulation coupling function with respect to $\delta A(w)$ (Figure 3c) also impacts the dynamic component (Figure 3e). To change the location of the nonlinearity in w space, we vary the constant e and measure the difference from the center of the nonlinearity, the inflection point, to the inflection point in $\delta A(w)$. This relative distance between the two inflection points has units of ms^{-1}. Figure 3e demonstrates that the magnitude of the dynamic component varies non-monotonically with the difference in inflection point and can be either a positive (warming) or negative (cooling) feedback depending on the structure of cloud–circulation coupling relative to the structure of the circulation change.

Using this toy model, we show that not only does a nonzero dynamic component require the climatological cloud–circulation coupling function to be nonlinear, but the size of the nonlinearity and its location in vertical velocity space influence the magnitude of the dynamic component, for a given change in circulation. The parameters of step-size and inflection point can be interpreted as representing aspects of climatological cloud–circulation coupling in models, that is, the sensitivity of CRE to circulation in the regime of weak vertical velocity (Figure 3b) and the relative position of this regime to a circulation change in vertical velocity space (Figure 3c), respectively. Therefore the characteristics of climatological cloud–circulation coupling, shown to be diverse among the RCEMIP models in Figures 2a and 2b, are crucial for determining how changes in circulation affect cloud feedbacks.

4. Dynamic Component Across Cloud-Resolving Models

The remainder of this paper will focus on the dynamic component of cloud feedbacks across the RCEMIP CRMs. We begin by quantifying the role of circulation changes in cloud feedbacks before assessing whether the intermodel spread in the dynamic component is controlled primarily by differences in circulation changes or differences in climatological cloud–circulation coupling across models (Section 4.1). This is followed by an investigation of how the dynamic component depends on bulk metrics of the atmospheric circulation (Section 4.2), with a focus on the physical processes controlling ascent fraction (Section 5).

4.1. Quantifying the Dynamic Component of the Cloud Feedback

Using the decomposition Equation 2, we calculate the total cloud feedback as well as the dynamic, thermodynamic and nonlinear components for both temperature differences (300 minus 295 K and 305 minus 300 K), and for the models listed in Table Appendix A (Figure 4). We verify that the sum of the feedback components [see (2)] is approximately equal to the total cloud "Cess"-type feedback calculated by taking the change in domain-mean cloud radiative effects between two simulations with different SSTs and dividing by the SST change. The multi-model mean difference between the two methods is $\sim$0.01 $\mathrm{Wm}^{-2}\,\mathrm{K}^{-1}$ for both the longwave and shortwave feedbacks.

The longwave thermodynamic component across the majority of models ranges from approximately -1 to $+1\ \mathrm{Wm}^{-2}\,\mathrm{K}^{-1}$, which is a larger range than the dynamic component (approximately -0.5 to $0.5\ \mathrm{Wm}^{-2}\,\mathrm{K}^{-1}$), though the dynamic component of MESONH falls outside of this range. Both the thermodynamic and dynamic components have a statistically significant ($p < 0.01$) correlation with the total (dynamic + thermodynamic + nonlinear) longwave cloud feedback (e.g., $r^2 = 0.95$, 0.53 for the longwave thermodynamic and dynamic components, respectively). The correlation between the total shortwave feedback and the dynamic component is less strong ($r^2 = 0.03$) and not statistically significant. A statistically significant correlation between the dynamic and thermodynamic components in the longwave ($r^2 = 0.42$) suggests that the processes determining the magnitude of the two components are not independent, though this does not apply in the shortwave ($r^2 = 0.00$ for the correlation between the thermodynamic and dynamic components). The net (shortwave + longwave) dynamic component, in contrast to the separate longwave and shortwave components, is generally small across the RCEMIP models (Figure 4) due to the cancellation of the longwave and shortwave dynamic components (e.g., Figure 2). An exception to this is the net cloud feedback for UCLA-CRM, which is large relative to the other models, due to a strongly positive shortwave feedback driven by the thermodynamic component. Opposing shortwave and

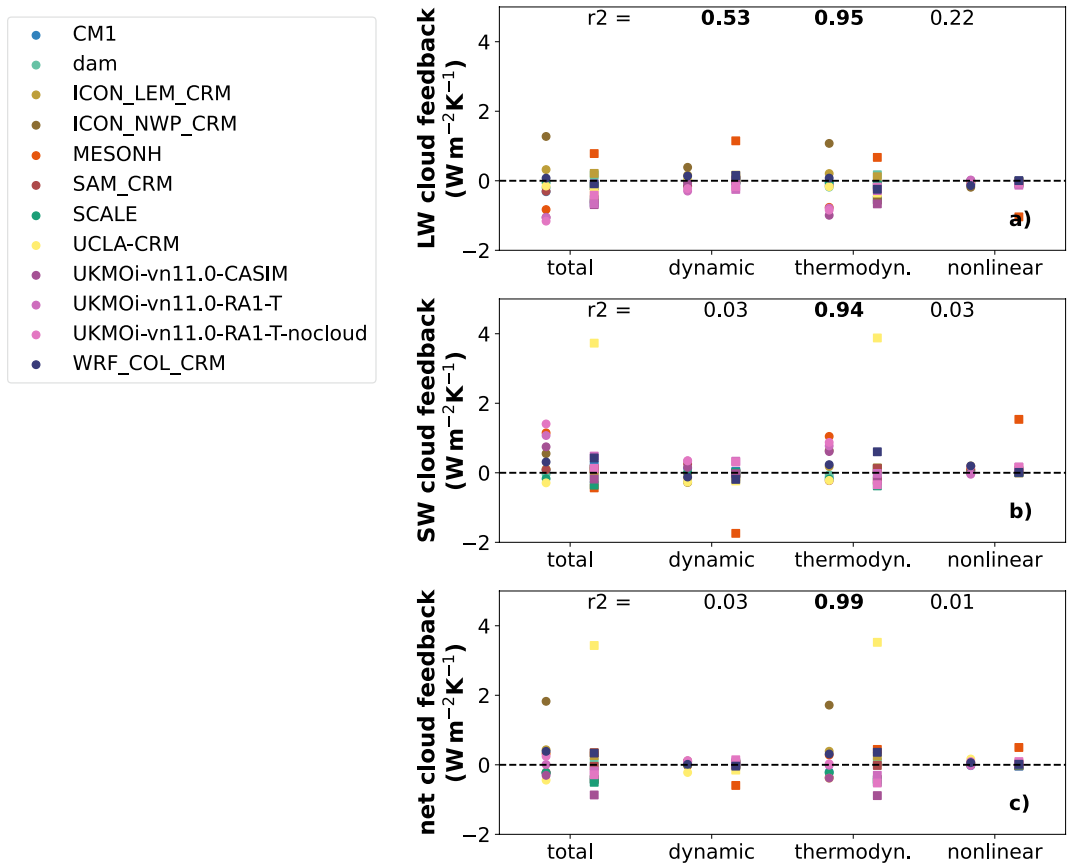

Figure 4. Total (a) longwave, (b) shortwave and (c) net cloud feedbacks, along with the dynamic, thermodynamic and nonlinear components as defined by Equation 2, for the RCEMIP cloud-resolving models. Feedbacks computed between the 295 and 300 K simulations (circles) and the 300 and 305 K simulations (squares) are shown. Numbers at the top of each panel indicate the Pearson correlation coefficient between the total cloud feedback and the various feedback components, across all models and both temperature changes. The correlations written in bold are statistically significant ($p < 0.01$).

longwave dynamic components of the tropical cloud feedback are also a feature of the tropics in CMIP5 (Byrne & Schneider, 2018), with longwave effects typically larger in magnitude in the multimodel mean.

In summary, the longwave and shortwave dynamic components are (a) substantial in magnitude compared to the total feedbacks; and (b) linked to differences in total cloud feedback across models, at least in the longwave. An immediate question arising from this analysis is whether intermodel differences in the dynamic component are primarily due to differences in climatological cloud–circulation coupling [that is, different $R(w)$ functions], or differences in circulation changes with warming [that is, different $\delta A(w)$]. To explore this question, we determine to what extent variations in the dynamic component across models can be reproduced using either the multimodel-mean cloud–circulation coupling function, $\overline{R(w)}$, or the multimodel-mean circulation change, $\overline{\delta A(w)}$. For each model, we calculate $\int_{-\infty}^{\infty} R(w)\overline{\delta A(w)}\mathrm{d}w$—the dynamic component assuming all models have the same change in circulation—and compare this to the full dynamic component (Figures 5a and 5c). We also compute $\int_{-\infty}^{\infty} \overline{R(w)} dA(w)\mathrm{d}w$—the dynamic component assuming all models have the same cloud–circulation coupling function (Figures 5b and 5d).

The intermodel spread in longwave and shortwave dynamic components is dominated by differences in circulation changes across models (Figures 5b and 5d) rather than differences in cloud–circulation coupling (Figures 5a and 5c). This suggests that while, as discussed in Section 3.1, a nonlinearity in $R(w)$ is an essential prerequisite for a nonzero dynamic component, and the structure of this nonlinearity and its location in vertical-velocity space affects the magnitude of the dynamic component (Figure 3), in the case of the models analyzed here, it is the diversity in the changes in circulation which largely controls the differences in the dynamic component. In

19422466, 2023, 5, Downloaded from https://agupubs.onlinelibrary.wiley.com/doi/10.1029/2022MS003516 by University Of St Andrews University, Wiley Online Library on [15/05/2023]. See the Terms and Conditions (https://onlinelibrary.wiley.com/terms-and-conditions) on Wiley Online Library for rules of use; OA articles are governed by the applicable Creative Commons License

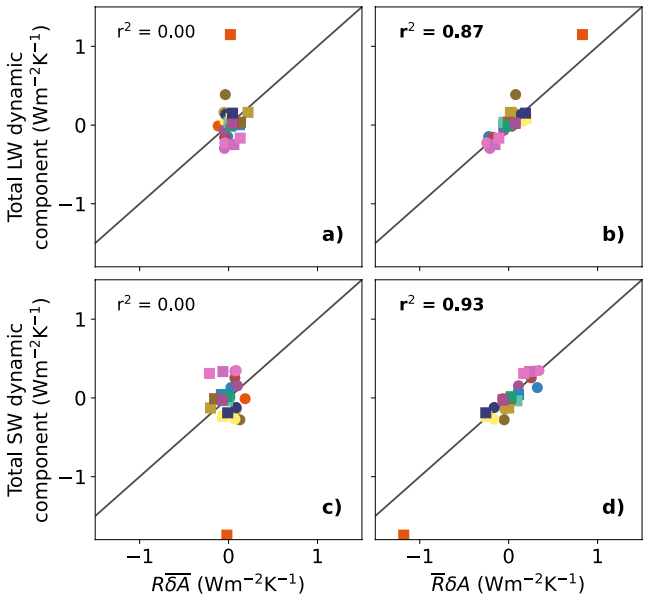

Figure 5. Panel (a) longwave and panel (c) shortwave dynamic components calculated using the multimodel-mean change in circulation $\left[\overline{\delta A(w)}\right]$ and model-specific cloud–circulation coupling functions $[R(w)]$, plotted against the full dynamic component calculated using Equation 2. Panels (b, d): As in panels (a, c) but here, for the x-axis, computing the longwave and shortwave dynamic components using the multimodel-mean cloud–circulation coupling function $\left[\overline{R(w)}\right]$ and the model-specific circulation changes $[\delta A(w)]$. Colors represent different models, corresponding to the legend in Figure 4. Dynamic component is calculated using the 295 and 300 K simulations (circles) and the 300 and 305 K simulations (squares). Numbers at the top of each panel indicate the Pearson correlation coefficient between the x and y axes, and are bold if statistically significant to $p < 0.01$.

the next section we explore the aspects of the circulation changes that determine the dynamic component of the cloud feedback.

4.2. Link Between Dynamic Component and Ascent Fraction

Differences in circulation changes across models drive the spread in the dynamic component. But changes in the full distribution of vertical velocity with warming are complex (Figure 2d) and difficult to interpret in straightforward physical terms. To gain insight into how circulation impacts cloud feedbacks, we focus on a particular bulk metric of the circulation: ascent fraction, α_{up}. Ascent fraction is defined as the fraction of the model domain ascending at 500 hPa and is closely related to the subsidence fraction, which has been analyzed extensively in RCE simulations (e.g., Becker & Wing, 2020; Cronin & Wing, 2017; Jenney et al., 2020; Wing et al., 2020). In these idealized simulations of a limited domain, in contrast to more realistic simulations on a sphere or the real atmosphere, an increase in tropical ascent fraction corresponds directly with a decrease in descent fraction, and vice versa. We find that fractional changes in ascent fraction vary significantly between models, from −3.2–+5.3% K^{-1}, with a multimodel mean value of 1.3% K^{-1}. That the majority of models simulate an increase in ascent fraction with warming is in contrast to GCMs, for example, those in the Coupled Model Intercomparison Project Phase 5 (CMIP5) (Su et al., 2019). Importantly, across models, there is a strong positive correlation between fractional changes in ascent fraction and the longwave dynamic component ($r^2 = 0.54$, Figure 6a); a strong negative correlation with the shortwave dynamic component ($r^2 = 0.50$ Figure 6b); and a weaker negative correlation with the total dynamic component ($r^2 = 0.31$, Figure 6c). We find similar, but less robust, relationships (not shown) if we use a measure of convective aggregation [specifically the organization index, Becker and Wing (2020)] in place of ascent fraction. The relationship between ascent fraction and longwave dynamic component is robust to different scales of spatial (Figure S3 in Supporting Information S1) and temporal averaging (Figure S4 in Supporting Information S1).

The statistical relationships between ascent fraction and the dynamic components arise from the tight coupling between changes in ascent fraction and high cloud fraction. In particular, fractional changes in high cloud fraction with warming are positively correlated with fractional changes in ascent fraction (Figure 7a), leading to a positive correlation with longwave dynamic components (Figure 7b) and a negative correlation with shortwave dynamic components (Figure 7c). The shortwave and longwave effects of high clouds approximately cancel one another (Kiehl, 1994), which offers a possible explanation as to why the net dynamic component—which is the sum of the longwave and shortwave dynamic components, both of which are linked to high cloud fraction (Figures 7b and 7c)—is small (Figure 4c). The positive correlations between high cloud fraction and ascent fraction have also been found in GCMs in the context of narrowing of the intertropical convergence zone (Su et al., 2017). It is noteworthy that this relationship exists in both the comprehensive global simulations of Su et al. (2017) and the idealized, limited-domain simulations we analyze here.

While there is a robust relationship between fractional changes in ascent fraction and high cloud fraction across the RCEMIP models, there are models which simultaneously have an expansion of the ascent region and a reduction in high cloud fraction as the relationship is offset from the origin (Figure 7a). Physically, this offset could arise, for example, from the stability iris mechanism (Bony et al., 2016) or from cloud lifetime changes with warming (Seeley et al., 2019); both of these effects could, in principle, influence high cloud fraction independent of changes in ascent fraction at 500 hPa. Indeed, the response of high cloud fraction to warming is not robust across the models: There are some models in which warming leads to an expansion of high cloud fraction, though the majority have a contraction. This is also true for the wider RCEMIP archive (Wing et al., 2020). The correlations between ascent fraction, longwave and shortwave dynamic components and low cloud fraction are weaker, and not statistically significant (Figure S5 in Supporting Information S1).

19422466, 2023, 5, Downloaded from https://agupubs.onlinelibrary.wiley.com/doi/10.1029/2022MS003516 by University Of St Andrews University, Wiley Online Library on [15/05/2023]. See the Terms and Conditions (https://onlinelibrary.wiley.com/terms-and-conditions) on Wiley Online Library for rules of use; OA articles are governed by the applicable Creative Commons License

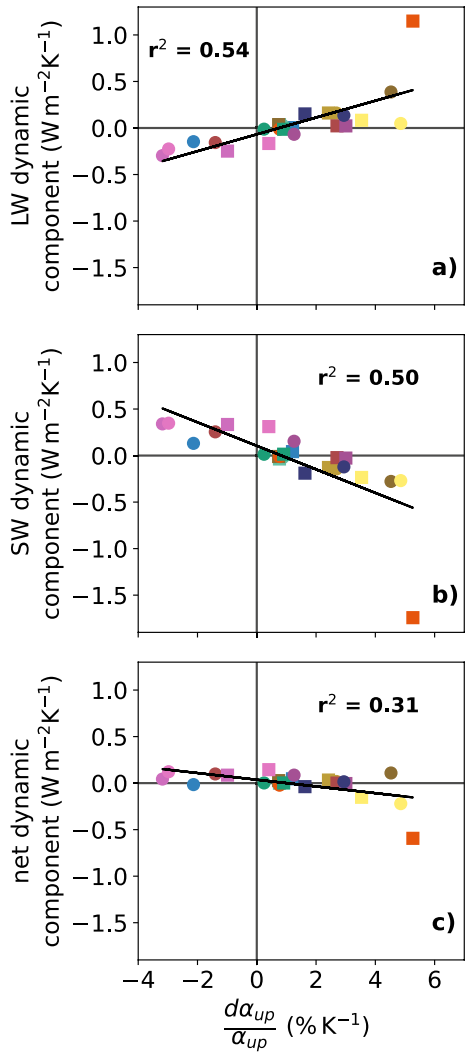

Figure 6. Fractional changes in ascent fraction between the 295 and 300 K simulations (circles) and the 300 and 305 K simulations (squares) versus the (a) longwave, (b) shortwave and (c) net (longwave plus shortwave) dynamic components. Colors represent different RCEMIP models, as in the legend of Figure 4. Inset text quotes the r^2 value for each panel (Pearson's correlation), with the text in bold if the correlation is statistically significant ($p < 0.01$).

The relationships between ascent fraction, high cloud fraction and the dynamic components of the cloud feedback can be interpreted in simple physical terms. For example, a decrease in ascent fraction is consistent with a decrease in the area of high clouds (Figure 7a), which in turn decreases the domain-mean shortwave cloud radiative effect and induces a positive shortwave cloud feedback (all else equal). While in our results the longwave and shortwave dynamic component of the cloud feedbacks largely cancel (Figure 6c), this conceptual picture is similar to ideas explored by Pierrehumbert (1995), Lindzen et al. (2001), Mauritsen and Stevens (2015), Bony et al. (2016) and others, who argued that a change in high cloud cover with warming could constitute an important feedback on the climate system. The possibility of a reduction in ascent area and high cloud fraction with warming has been linked to the self-aggregation of convection, which is associated with a reduction of a high cloud cover and an increase in radiative cooling to space (Wing, 2019). However, it should be noted that the dynamic component of the cloud feedback captures all effects due to changes in circulation, not just those associated with self-aggregation, or indeed more generally those associated with a reduction of ascent fraction.

5. Physical Processes Controlling Ascent Fraction

The strong link between the dynamic components of the cloud feedback and ascent fraction motivates the questions: What physical processes control ascent fraction in a changing climate? And can these processes account for the spread in dynamic components across RCEMIP models? The remainder of the paper will focus on addressing these two questions.

5.1. Connecting Ascent Fraction to Diabatic Heating and Static Stability

To understand the processes influencing ascent fraction—and therefore the dynamic components of the cloud feedback—we first invoke the energy and mass budgets of the atmosphere. In particular, we follow the framework of Jenney et al. (2020) who derive an expression for the ascent fraction in terms of static stability and the diabatic heating rates in ascending and descending regimes. [A similar approach was taken by Byrne and Schneider (2016a, 2016b) to understand the processes controlling the width of the intertropical convergence zone]. Here we outline a version of the Jenney et al. (2020) framework in pressure coordinates, starting with the steady-state energy budgets averaged over ascending regions (denoted using the subscript "*up*") and descending regions (subscript "*dn*") separately:

$$-\omega_{up} S_{up} = Q_{up} = Q^c_{up} + Q^r_{up} \tag{4}$$

$$-\omega_{dn} S_{dn} = Q_{dn} = Q^c_{dn} + Q^r_{dn}, \tag{5}$$

where all quantities are means over the fraction of the domain which is either ascending Equation 4 or descending at 500 hPa Equation 5; ω is the vertical velocity in pressure coordinates; Q is the diabatic heating rate, consisting of radiative (Q^r) and non-radiative contributions (Q^c); and $S = -(T/\theta) \times \partial\theta/\partial p$ is the static stability in pressure coordinates (T and θ represent temperature and potential temperature, respectively, and p is pressure), and all variables are evaluated at 500 hPa. Note that the "weak temperature gradient" (WTG) approximation—which suggests free-tropospheric temperature gradients in the tropics are weak owing to the small effects of planetary rotation at low latitudes (Charney, 1963; Sobel & Bretherton, 2000)—has been invoked in the derivations of Equations 4 and 5, leading to the horizontal advection terms being dropped. The WTG approximation is expected to be applicable to the simulations being analyzed here, which have zero rotation. Indeed, in the multimodel mean,

19422466, 2023, 5, Downloaded from https://agupubs.onlinelibrary.wiley.com/doi/10.1029/2022MS003516 by University Of St Andrews University, Wiley Online Library on [15/05/2023]. See the Terms and Conditions (https://onlinelibrary.wiley.com/terms-and-conditions) on Wiley Online Library for rules of use; OA articles are governed by the applicable Creative Commons License

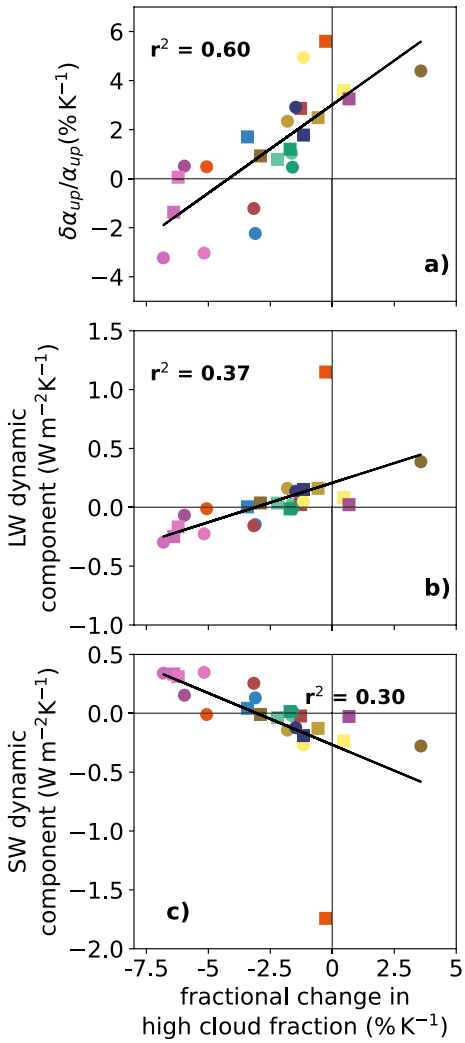

Figure 7. Fractional change in high cloud fraction with fractional changes in (a) ascent fraction, (b) longwave dynamic component and (c) shortwave dynamic component. Colors indicate different models, as in Figure 4. Inset text gives the Pearson's r^2 value, with the text in bold if statistically significant ($p < 0.01$) for the correlation between x-axis and fractional change in high cloud fraction (black). Cloud fraction is calculated at each model level following the method in Wing et al. (2020), using a threshold value of cloud condensate. We calculate the mean cloud profile for each model, and take the high cloud fraction at the peak of the profile above 500 hPa.

horizontal temperature advection at 500 hPa is orders of magnitude smaller than vertical advection (0.0016 K s^{-1} compared to 0.24 K s^{-1}), supporting the use of the WTG approximation in deriving Equations 4 and 5. We expect that in descending regions, with little precipitation, the dominant diabatic term in the energy budget is radiative cooling. In contrast, while ascending regions also cool radiatively, latent heat release is more influential (Neelin, 1988), leading to a net positive, or warming, diabatic term (Figure S6 in Supporting Information S1).

In steady state, the mass budget of the atmosphere can be expressed as:

$$\omega_{up}\alpha_{up} = -\omega_{dn}\alpha_{dn}, \tag{6}$$

where $\alpha_{dn} = 1 - \alpha_{up}$ is the fraction of the domain with descending air at 500 hPa: In simple terms, Equation 6 states that "what goes up must come down." Combining the energy and mass budgets, an expression for the ascent fraction as a function of diabatic heating rates and static stabilities in the ascent and descent regions can be derived:

$$\alpha_{up} = \frac{1}{1 - \gamma(Q_{up}/Q_{dn})}, \tag{7}$$

where $\gamma \equiv S_{dn}/S_{up}$ is the ratio of the static stabilities in the descent and ascent regions. Due to the WTG approximation we expect this ratio to be approximately 1 in the free troposphere. Indeed we find that for the 295 K simulations, γ at 500 hPa ranges from 0.87 to 1.07 across models, with a multimodel mean of 0.97. This expression for α_{up} holds for much of the troposphere (Jenney et al., 2020) and in the following analyses we focus on the 500 hPa level.

5.2. Processes Controlling Ascent Fraction

We have demonstrated that there exists a strong relationship between ascent fraction at 500 hPa and the dynamic components of the cloud feedback (Figure 6). We now apply Equations 4 and 5 to understand the processes determining ascent fraction at that level. The diabatic temperature tendency due to radiative processes, Q^r, is a standard output for the RCEMIP simulations; we compute the non-radiative diabatic temperature tendency, Q^c, as a residual from the energy budgets Equations 4 and 5.

First, we verify that the expression Equation 7 for α_{up}—derived using the energy and mass budgets and invoking the WTG approximation—holds at 500 hPa. We find that despite a small tendency to overestimate α_{up}, Equation 7 provides a good approximation to ascent fraction across all the models (Figure S7a in Supporting Information S1). Fractional changes in simulated and approximated α_{up} between simulations, which we use in our subsequent analyses, are also very similar (Figure S7b in Supporting Information S1).

Next we linearize Equation 7 to explore how fractional changes in ascent fraction depend on energetic processes in the atmosphere, namely diabatic heating rates and static stability:

$$\frac{\delta\alpha_{up}}{\alpha_{up}} \approx \underbrace{\frac{\gamma}{1 - \gamma\frac{Q_{up}}{Q_{dn}}}\frac{Q_{up}}{Q_{dn}}}_{-\beta_1}\left[\frac{\delta Q_{up}}{Q_{up}} - \frac{\delta Q_{dn}}{Q_{dn}}\right]. \tag{8}$$

To obtain Equation 8, we neglect fractional changes in $\gamma = S_{dn}/S_{up}$. This is justified again by the WTG approximation, which constrains the static stabilities in the ascent and descent regions to be similar, as discussed above.

19422466, 2023, 5, Downloaded from https://agupubs.onlinelibrary.wiley.com/doi/10.1029/2022MS003516 by University Of St Andrews University, Wiley Online Library on [15/05/2023]. See the Terms and Conditions (https://onlinelibrary.wiley.com/terms-and-conditions) on Wiley Online Library for rules of use; OA articles are governed by the applicable Creative Commons License

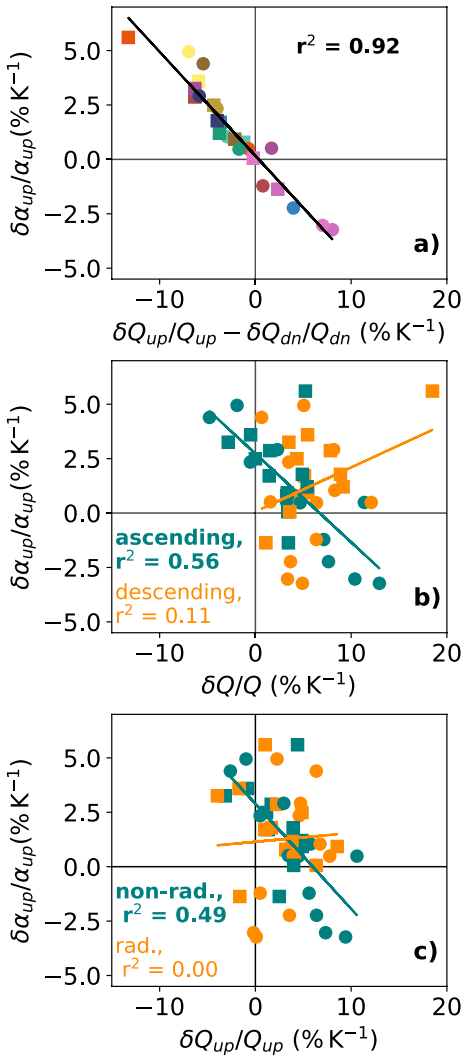

Figure 8. Relationships between fractional changes in ascent fraction and (a) $\delta Q_{up}/Q_{up}$–$\delta Q_{dn}/Q_{dn}$; (b) fractional changes in ascent region diabatic heating rate ($\delta Q_{up}/Q_{up}$, teal) and descent region diabatic heating rate ($\delta Q_{dn}/Q_{dn}$, orange); and (c) as in panel (b), but for ascent region radiative ($\delta Q^r_{up}/Q^r_{up}$) and non-radiative ($\delta Q^c_{up}/Q^c_{up}$) diabatic heating rates. Colors in panel (a) indicate different models, as in Figure 4. Inset text quotes the Pearson's r^2 values, with the text in bold if the correlation is statistically significant ($p < 0.01$).

The approximation Equation 8 broadly captures the simulated fractional changes in ascent fraction across models (Figure S8a in Supporting Information S1); accounting for changes in γ improves the approximation marginally (Figure S8b in Supporting Information S1).

Equation 8 suggests that the response of ascent fraction to warming, and therefore the dynamic components of the cloud feedback, are tightly coupled to sources of diabatic heating in the atmosphere. In particular, Equation 8 highlights that a key control on ascent fraction is the contrast in fractional changes in diabatic heating between ascending and descending regions. If diabatic heating increases in magnitude with warming at the same fractional rate in ascending and descending regions, the ascent fraction would not change. Analogously, a larger fractional increase in diabatic heating in the ascending region relative to the descending regions implies a narrowing of ascent and vice versa. Note that the prefactor, $-\beta_1$, multiplying fractional changes in diabatic heating [see (8)] is a function of the climatological atmospheric state and is negative for all models analyzed (i.e., β_1 is positive).

We examine how contrasting fractional changes in diabatic heating influence changes in ascent fraction across the RCEMIP models (Figure 8). As expected based on the approximation Equation 8, there is a strong relationship between fractional changes in ascent fraction and the difference in fractional changes in diabatic heating between ascending and descending regions (Figure 8a). The intermodel spread in ascent fraction changes is also linked to diabatic heating changes in the ascending region ($r^2 = 0.56$; see Figure 8b), but there is no relationship to diabatic heating changes in the descending region ($r^2 = 0.11$).

The relationship between ascent fraction and diabatic heating can be interpreted in the following way: An increase in SST leads to a positive fractional change in Q_{dn} (i.e., Q_{dn} becomes more negative) in all models (Figure 8b), consistent with increased radiative cooling from a warmer, moister atmosphere (Pendergrass & Hartmann, 2014). This effect, all else being equal, would drive an increase in ascent fraction according to Equation 8. However, changes in Q_{up} with SST are less consistent across models: while the majority of pairs of model simulations (18 of the 22) have a positive fractional change in Q_{up}, corresponding to a decrease in α_{up} should no other changes occur, a minority of simulation pairs show a fractional decrease in Q_{up}. The relative sizes of fractional changes in Q_{up} and Q_{dn} determine the change in α_{up}, and only six of the simulation pairs have a sufficiently positive fractional change in Q_{up} to overcome the change in Q_{dn} (Figure 8a). Therefore, while relative changes in Q_{up} versus Q_{dn} determine changes in α_{up}, the spread between models of fractional changes in α_{up}, and therefore the dynamic component of the cloud feedback, are largely due to variations between models in the response of Q_{up}. This may arise from simulated convective and cloud processes in ascending regions being less consistent across RCEMIP models than the clear-sky processes in descending regions (see, e.g., the smaller spread in clear-sky feedback parameter in Becker and Wing (2020)).

There are similarities between our results and the work of Su et al. (2019), who found that while mean descending vertical velocity, or descent rate, changes in CMIP5 models were largely consistent across models, there was a far larger diversity in mean ascending vertical velocity, or ascent rate, changes in response to warming. While not directly comparable with our results, as we focus on changes in heating rates rather than descent/ascent rates with warming, it is of interest that in both studies it is processes within the ascending regions which most strongly affect intermodel spread ascent fraction response.

19422466, 2023, 5, Downloaded from https://agupubs.onlinelibrary.wiley.com/doi/10.1029/2022MS003516 by University Of St Andrews University, Wiley Online Library on [15/05/2023]. See the Terms and Conditions (https://onlinelibrary.wiley.com/terms-and-conditions) on Wiley Online Library for rules of use; OA articles are governed by the applicable Creative Commons License

19422466, 2023, 5, Downloaded from https://agupubs.onlinelibrary.wiley.com/doi/10.1029/2022MS003516 by University Of St Andrews University, Wiley Online Library on [15/05/2023]. See the Terms and Conditions (https://onlinelibrary.wiley.com/terms-and-conditions) on Wiley Online Library for rules of use; OA articles are governed by the applicable Creative Commons License

5.3. Radiative Versus Non-radiative Diabatic Heating

To further probe the processes driving intermodel spread in ascent fraction changes, we divide the total diabatic heating in ascent regions into radiative and non-radiative components (i.e., $Q_{up} = Q^r_{up} + Q^c_{up}$):

$$\frac{\delta Q_{up}}{Q_{up}} = \underbrace{\frac{Q^c_{up}}{Q^c_{up} + Q^r_{up}}}_{\beta_2} \frac{\delta Q^c_{up}}{Q^c_{up}} - \underbrace{-\frac{Q^r_{up}}{Q^c_{up} + Q^r_{up}}}_{\beta_3} \frac{\delta Q^r_{up}}{Q^r_{up}}, \tag{9}$$

where both β_2 and β_3 are both positive as Q^c_{up} (largely driven by latent heating, a positive term) is positive, Q^r_{up} is negative (from radiative cooling) and $|Q^c_{up}| > |Q^r_{up}|$ (Figure S5b in Supporting Information S1). Substituting Equation 9 into Equation 8 leads to:

$$\frac{\delta \alpha_{up}}{\alpha_{up}} = -\beta_1 \left[\beta_2 \frac{\delta Q^c_{up}}{Q^c_{up}} - \beta_3 \frac{\delta Q^r_{up}}{Q^r_{up}} - \frac{\delta Q_{dn}}{Q_{dn}} \right]. \tag{10}$$

Equation 10 again broadly captures variations in the fractional change in ascent fraction (Figure S8c in Supporting Information S1) and highlights how both radiative and non-radiative diabatic heating in ascending regions influence ascent fraction, though the relative importance of each term is unclear. We find a statistically significant correlation between fractional changes in non-radiative diabatic heating and fractional changes in ascent fraction ($r^2 = 0.49$; Figure 8c), but no significant correlation with radiative heating changes ($r^2 = 0.00$). This suggests that it is the non-radiative diabatic heating response to warming in the ascent region which is most strongly linked to intermodel differences in fractional changes in ascent fraction.

To what extent can a similar argument be made to explain the differing roles of circulation changes in cloud feedbacks across models? Fractional changes in the diabatic heating contrast between ascending and descending regions correlate significantly with the spread in longwave dynamic component ($r^2 = 0.63$, Figure S9a in Supporting Information S1), despite the large dynamic component, relative to other models, of MESONH. The dynamic component is negatively correlated with these terms: If fractional changes in Q_{up} increase relative to fractional changes in Q_{dn}, ascent fraction decreases and the longwave component of the cloud feedback is negative.

The next logical question, following the analysis above, is which non-radiative processes may be contributing to the spread in Q^c_{up} and thus to differing ascent fraction responses. Non-radiative diabatic heating is composed of contributions from latent heating, detrainment and dry static energy transport due to turbulence (Jenney et al., 2020). We do not isolate the roles of these individual non-radiative diabatic heating processes here, given the required data are not available in the RCEMIP archive, but this would be an interesting avenue for future research. Another interesting question is whether intermodel differences in how non-radiative heating changes with warming arise from differing cloud physics, surface fluxes or other factors. Schiro et al. (2019) explore this question by perturbing convective and cloud parameterizations in a GCM to recreate the spread in ascent fraction change across the CMIP5 ensemble, and find that convective parameterizations are key to explaining differing ascent-fraction responses.

6. Discussion

Cloud feedbacks remain one of the largest sources of uncertainty in climate projections. The role of circulation changes in modulating cloud feedbacks is limited in GCMs when spatially averaged over large scales, but on regional scales circulation changes can couple strongly to cloud feedbacks, particularly in the tropics (Byrne & Schneider, 2018). Beyond the current generation of global models, in high-resolution models that explicitly simulate deep convection and in the real Earth system, the influence of circulation on cloud feedbacks is an open question.

Here we investigate cloud–circulation coupling using idealized cloud-resolving simulations in RCE (Wing et al., 2018, 2020). Cloud feedbacks are decomposed into dynamic and thermodynamic components following Bony et al. (2004) in order to directly quantify the role of circulation changes (i.e., the dynamic component). Across the RCEMIP models, we find a wide range of dynamic components, some of which contribute substantially to the total cloud feedback. Some models have a strong positive longwave dynamic component, some have a strong negative longwave dynamic component, and some have a small dynamic component. In general, the shortwave dynamic component for a given model is of similar magnitude and opposite sign to the longwave dynamic component.

19422466, 2023, 5, Downloaded from https://agupubs.onlinelibrary.wiley.com/doi/10.1029/2022MS003516 by University Of St Andrews University, Wiley Online Library on [15/05/2023]. See the Terms and Conditions (https://onlinelibrary.wiley.com/terms-and-conditions) on Wiley Online Library for rules of use; OA articles are governed by the applicable Creative Commons License

We establish a strong link between the dynamic component of the cloud feedback and the degree to which the ascent region narrows or widens with warming. Models which have the strongest narrowing of ascent with warming also have the strongest longwave and shortwave dynamic components of the cloud feedback, due to decreases in high cloud fraction. We identify similar relationships between changes in high cloud fraction and ascent fraction as have been found in comprehensive global simulations, such as CMIP5 (Su et al., 2017). The dynamic components and changes in ascent fraction are linked—via the energy and mass budgets of the atmosphere—to diabatic heating rates in ascending and descending regions. Specifically, intermodel differences in how ascent fraction changes with warming are coupled to differences in non-radiative diabatic processes, including latent heating, in ascending regions. However, a stronger predictor of ascent region narrowing or expansion—and therefore a strong predictor of the dynamic component—is the contrast in diabatic heating changes between ascending and descending regions.

Our study highlights a number of interesting possibilities for further research. First, a key question is the degree to which different non-radiative diabatic processes—including latent heat release, convective entrainment and cloud microphysics—drive the response of ascent fraction and high-cloud fraction to warming. Also, what is the effect of a large-scale circulation, for example, driven by SST gradients, on the relationships between cloud feedbacks and circulation examined here? And finally, does the substantial influence of circulation on clouds found in tropical high-resolution models have implications for estimates of cloud feedbacks and climate sensitivity in global models? While we focus here on high-resolution simulations in RCE, an interesting avenue for further study would be to explore the effects of circulation on cloud feedbacks in global models under RCE. This would allow for a more direct assessment of the role of model resolution in shaping the dynamic component of the cloud feedbacks. That non-radiative processes play a greater role in ascent fraction changes across models in the long-channel, limited-domain, fixed SST simulations analyzed here appears to contradict the findings of Voigt and Shaw (2015), who found that radiative processes were crucial to ascent fraction widening/narrowing with warming in two fixed-SST global aquaplanet models. Understanding the processes driving these differing behaviors in different model configurations would be an interesting avenue for future research. Another difference between the models used here and global coupled models is the contrasting effects of warming on ascent fraction: use of GCM simulations in the RCEMIP archive may provide insight in how these contrasting behaviors can be reconciled. Pursuing these questions, perhaps through analyses of observations and a hierarchy of models, will further build understanding of the role of cloud–circulation coupling in the climate system.

Appendix A

See Table A1

Table A1
The RCEMIP Models Analyzed in This Study

Full name	Abbreviation
Cloud Model 1, cm1r19.6	CM1
Das Atmosphaerische Modell	dam
ICOsahedral Nonhydrostatic-2.3.00, LEM config.	ICON_LEM_CRM
ICOsahedral Nonhydrostatic-2.3.00, NWP config.	ICON_NWP_CRM
Meso-NH v5.4.1	MESONH
System for Atmospheric Modeling 6.11.2	SAM_CRM
SCALE v5.2.5	SCALE
UCLA Large-Eddy Simulation model	UCLA_CRM
UK Met Office Idealized Model v11.0 — CASIM	UKMOi-vn11.0-CASIM
UK Met Office Idealized Model v11.0 — RA1-T	UKMOi-vn11.0-RA1-T
UK Met Office Idealized Model v11.0 — RA1-T	UKMOi-vn11.0-RA1-T-nocloud
Weather Research and Forecasting model v3.5.1	WRF_COL_CRM

Note. For more details about individual models see Wing et al. (2020).

Data Availability Statement

All RCEMIP data used in this study is available at https://swiftbrowser.dkrz.de/public/dkrz_70a517a8-039d-4a1b-a30d-841923f8bc7a/RCEMIP/ (RCEMIP, 2020; Wing et al., 2018, 2020). Analysis scripts are available here: https://github.com/Climate-Dynamics-Lab/Mackie_Byrne_2022 (Mackie, 2023).

Acknowledgments
We acknowledge funding from the UK Natural Environment Research Council (Grant NE/T006269/1). We thank the German Climate Computing Center (DKRZ) for hosting the standardized RCEMIP data. We thank the reviewers for their helpful feedback. We further thank Peter Hill, Chris Holloway, Hugo Lambert, Monisha Natchair, Levi Silvers, Mark Webb, and Allison Wing for helpful discussions and suggestions.

References

Bao, J., Sherwood, S. C., Colin, M., & Dixit, V. (2017). The robust relationship between extreme precipitation and convective organization in idealized numerical modeling simulations. *Journal of Advances in Modeling Earth Systems*, *9*(6), 2291–2303. https://doi.org/10.1002/2017MS001125

Becker, T., & Wing, A. A. (2020). Understanding the extreme spread in climate sensitivity within the radiative-convective equilibrium model intercomparison project. *Journal of Advances in Modeling Earth Systems*, *12*(10), e2020MS002165. https://doi.org/10.1029/2020MS002165

Bony, S., Colman, R., Kattsov, V. M., Allan, R. P., Bretherton, C. S., Dufresne, J., et al. (2006). How well do we understand and evaluate climate change feedback processes? *Journal of Climate*, *19*(15), 3445–3482. https://doi.org/10.1175/JCLI3819.1

Bony, S., & Dufresne, J.-L. (2005). Marine boundary layer clouds at the heart of tropical cloud feedback uncertainties in climate models. *Geophysical Research Letters*, *32*(20), L20806. https://doi.org/10.1029/2005GL023851

Bony, S., Dufresne, J.-L., Le Treut, H., Morcrette, J.-J., & Senior, C. (2004). On dynamic and thermodynamic components of cloud changes. *Climate Dynamics*, *22*(2), 71–86. https://doi.org/10.1007/s00382-003-0369-6

Bony, S., Stevens, B., Coppin, D., Becker, T., Reed, K. A., Voigt, A., & Medeiros, B. (2016). Thermodynamic control of anvil cloud amount. *Proceedings of the National Academy of Sciences of the United States of America*, *113*(32), 8927–8932. https://doi.org/10.1073/pnas.1601472113

Bony, S., Stevens, B., Frierson, D. M. W., Jakob, C., Kageyama, M., Pincus, R., et al. (2015). Clouds, circulation and climate sensitivity. *Nature Geoscience*, *8*(4), 261–268. https://doi.org/10.1038/ngeo2398

Bretherton, C. S., Blossey, P. N., & Khairoutdinov, M. (2005). An energy-balance analysis of deep convective self-aggregation above uniform SST. *Journal of the Atmospheric Sciences*, *62*(12), 4273–4292. https://doi.org/10.1175/JAS3614.1

Byrne, M. P., & Schneider, T. (2016a). Energetic constraints on the width of the intertropical convergence zone. *Journal of Climate*, *29*(13), 4709–4721. https://doi.org/10.1175/JCLI-D-15-0767.1

Byrne, M. P., & Schneider, T. (2016b). Narrowing of the ITCZ in a warming climate: Physical mechanisms. *Geophysical Research Letters*, *43*(21), 11350–11357. https://doi.org/10.1002/2016gl070396

Byrne, M. P., & Schneider, T. (2018). Atmospheric dynamics feedback: Concept, simulations, and climate implications. *Journal of Climate*, *31*(8), 3249–3264. https://doi.org/10.1175/JCLI-D-17-0470.1

Ceppi, P., Brient, F., Zelinka, M. D., & Hartmann, D. L. (2017). Cloud feedback mechanisms and their representation in global climate models. *WIREs Climate Change*, *8*(4), e465. https://doi.org/10.1002/wcc.465

Cess, R. D., & Potter, G. L. (1988). A methodology for understanding and intercomparing atmospheric climate feedback processes in general circulation models. *Journal of Geophysical Research*, *93*(D7), 8305–8314. https://doi.org/10.1029/JD093iD07p08305

Charney, J. G. (1963). A note on large-scale motions in the tropics. *Journal of the Atmospheric Sciences*, *20*(6), 607–609. https://doi.org/10.1175/1520-0469(1963)020⟨0607:ANOLSM⟩2.0.CO;2

Cronin, T. W., & Wing, A. A. (2017). Clouds, circulation, and climate sensitivity in a radiative-convective equilibrium channel model. *Journal of Advances in Modeling Earth Systems*, *9*(8), 2883–2905. https://doi.org/10.1002/2017MS001111

Hartmann, D. L., & Larson, K. (2002). An important constraint on tropical cloud—Climate feedback. *Geophysical Research Letters*, *29*(20), 12-1–12-4. https://doi.org/10.1029/2002GL015835

Hartmann, D. L., Moy, L. A., & Fu, Q. (2001). Tropical convection and the energy balance at the top of the atmosphere. *Journal of Climate*, *14*(24), 4495–4511. https://doi.org/10.1175/1520-0442(2001)014⟨4495:TCATEB⟩2.0.CO;2

Held, I. M., Hemler, R. S., & Ramaswamy, V. (1993). Radiative-convective equilibrium with explicit two-dimensional moist convection. *Journal of the Atmospheric Sciences*, *50*(23), 3909–3927. https://doi.org/10.1175/1520-0469(1993)050⟨3909:RCEWET⟩2.0.CO;2

Holloway, C. E., & Woolnough, S. J. (2016). The sensitivity of convective aggregation to diabatic processes in idealized radiative-convective equilibrium simulations. *Journal of Advances in Modeling Earth Systems*, *8*(1), 166–195. https://doi.org/10.1002/2015MS000511

Jenney, A. M., Randall, D. A., & Branson, M. D. (2020). Understanding the response of tropical ascent to warming using an energy balance framework. *Journal of Advances in Modeling Earth Systems*, *12*(6), e2020MS002056. https://doi.org/10.1029/2020MS002056

Kiehl, J. (1994). On the observed near cancellation between longwave and shortwave cloud forcing in tropical regions. *Journal of Climate*, *7*(4), 559–565. https://doi.org/10.1175/1520-0442(1994)007⟨0559:OTONCB⟩2.0.CO;2

Lindzen, R. S., Chou, M.-D., & Hou, A. Y. (2001). Does the Earth have an adaptive infrared iris? *Bulletin of the American Meteorological Society*, *82*(3), 417–432. https://doi.org/10.1175/1520-0477(2001)082⟨0417:DTEHAA⟩2.3.CO;2

Lutsko, N. J. (2018). The relationship between cloud radiative effect and surface temperature variability at El Niño-Southern Oscillation frequencies in CMIP5 models. *Geophysical Research Letters*, *45*(19), 10599–10608. https://doi.org/10.1029/2018GL079236

Mackie, A. (2023). Climate-Dynamics-Lab/Mackie_Byrne_2022: March 02, 2023 release (version 4). [Software]. Zenodo. https://zenodo.org/badge/latestdoi/554694313

Mauritsen, T., & Stevens, B. (2015). Missing iris effect as a possible cause of muted hydrological change and high climate sensitivity in models. *Nature Geoscience*, *8*(5), 346–351. https://doi.org/10.1038/ngeo2414

Muller, C. J., & Held, I. M. (2012). Detailed investigation of the self-aggregation of convection in cloud-resolving simulations. *Journal of the Atmospheric Sciences*, *69*(8), 2551–2565. https://doi.org/10.1175/JAS-D-11-0257.1

Neelin, J. D. (1988). A simple model for surface stress and low-level flow in the tropical atmosphere driven by prescribed heating. *Quarterly Journal of the Royal Meteorological Society*, *114*(481), 747–770. https://doi.org/10.1175/2008JCLI2303.1

Pendergrass, A. G., & Hartmann, D. L. (2014). The atmospheric energy constraint on global-mean precipitation change. *Journal of Climate*, *27*(2), 757–768. https://doi.org/10.1175/JCLI-D-13-00163.1

Pendergrass, A. G., Reed, K. A., & Medeiros, B. (2016). The link between extreme precipitation and convective organization in a warming climate: Global radiative-convective equilibrium simulations. *Geophysical Research Letters*, *43*(21), 11445–11452. https://doi.org/10.1002/2016GL071285

19422466, 2023, 5, Downloaded from https://agupubs.onlinelibrary.wiley.com/doi/10.1029/2022MS003516 by University Of St Andrews University, Wiley Online Library on [15/05/2023]. See the Terms and Conditions (https://onlinelibrary.wiley.com/terms-and-conditions) on Wiley Online Library for rules of use; OA articles are governed by the applicable Creative Commons License

Pierrehumbert, R. T. (1995). 05). Thermostats, radiator fins, and the local runaway greenhouse. *Journal of the Atmospheric Sciences*, *52*(10), 1784–1806. https://doi.org/10.1175/1520-0469(1995)052⟨1784:TRFATL⟩2.0.CO;2

RCEMIP. (2020). The radiative-convective equilibrium project [Dataset]. RCEMIP. Retrieved from https://swiftbrowser.dkrz.de/public/dkrz_70a517a8-039d-4a1b-a30d-841923f8bc7a/RCEMIP/

Romps, D. M., & Kuang, Z. (2011). A transilient matrix for moist convection. *Journal of the Atmospheric Sciences*, *68*(9), 2009–2025. https://doi.org/10.1175/2011JAS3712.1

Schiro, K. A., Su, H., Wang, Y., Langenbrunner, B., Jiang, J. H., & Neelin, J. D. (2019). Relationships between tropical ascent and high cloud fraction changes with warming revealed by perturbation physics experiments in CAM5. *Geophysical Research Letters*, *46*(16), 10112–10121. https://doi.org/10.1029/2019GL083026

Seeley, J. T., Jeevanjee, N., Langhans, W., & Romps, D. M. (2019). Formation of tropical anvil clouds by slow evaporation. *Geophysical Research Letters*, *46*(1), 492–501. https://doi.org/10.1029/2018gl080747

Sherwood, S. C., Bony, S., & Dufresne, J.-L. (2014). Spread in model climate sensitivity traced to atmospheric convective mixing. *Nature*, *505*(7481), 37–42. https://doi.org/10.1038/nature12829

Silvers, L. G., Reed, K. A., & Wing, A. A. (2023). The response of the large-scale tropical circulation to warming. *Journal of Advances in Modeling Earth Systems*, *15*(3), e2021MS002966. https://doi.org/10.1029/2021MS002966

Singh, M. S., & O'Gorman, P. A. (2015). Increases in moist-convective updraught velocities with warming in radiative-convective equilibrium. *Quarterly Journal of the Royal Meteorological Society*, *141*(692), 2828–2838. https://doi.org/10.1002/qj.2567

Sobel, A. H., & Bretherton, C. S. (2000). Modeling tropical precipitation in a single column. *Journal of Climate*, *13*(24), 4378–4392. https://doi.org/10.1175/1520-0442(2000)013⟨4378:MTPIAS⟩2.0.CO;2

Soden, B. J., Held, I. M., Colman, R., Shell, K. M., Kiehl, J. T., & Shields, C. A. (2008). Quantifying climate feedbacks using radiative kernels. *Journal of Climate*, *21*(14), 3504–3520. https://doi.org/10.1175/2007JCLI2110.1

Su, H., Jiang, J. H., Neelin, J. D., Shen, T. J., Zhai, C., Yue, Q., et al. (2017). Tightening of tropical ascent and high clouds key to precipitation change in a warmer climate. *Nature Communications*, *8*(1), 15771. https://doi.org/10.1038/ncomms15771

Su, H., Zhai, C., Jiang, J. H., Wu, L., Neelin, J. D., & Yung, Y. L. (2019). A dichotomy between model responses of tropical ascent and descent to surface warming. *Npj Climate and Atmospheric Science*, *2*(8), 8. https://doi.org/10.1038/s41612-019-0066-8

Voigt, A., & Shaw, T. A. (2015). Circulation response to warming shaped by radiative changes of clouds and water vapour. *Nature Geoscience*, *8*(2), 102–106. https://doi.org/10.1038/ngeo2345

Webb, M. J., Andrews, T., Bodas-Salcedo, A., Bony, S., Bretherton, C. S., Chadwick, R., et al. (2017). The cloud feedback model intercomparison project (CFMIP) contribution to CMIP6. *Geoscientific Model Development*, *10*(1), 359–384. https://doi.org/10.5194/gmd-10-359-2017

Wing, A. A. (2019). Self-aggregation of deep convection and its implications for climate. *Current Climate Change Reports*, *5*(1), 1–11. https://doi.org/10.1007/s40641-019-00120-3

Wing, A. A., & Cronin, T. W. (2016). Self-aggregation of convection in long channel geometry. *Quarterly Journal of the Royal Meteorological Society*, *142*(694), 1–15. https://doi.org/10.1002/qj.2628

Wing, A. A., & Emanuel, K. A. (2014). Physical mechanisms controlling self-aggregation of convection in idealized numerical modeling simulations. *Journal of Advances in Modeling Earth Systems*, *6*(1), 59–74. https://doi.org/10.1002/2013MS000269

Wing, A. A., Reed, K. A., Satoh, M., Stevens, B., Bony, S., & Ohno, T. (2018). Radiative–convective equilibrium model intercomparison project. *Geoscientific Model Development*, *11*(2), 793–813. https://doi.org/10.5194/gmd-11-793-2018

Wing, A. A., Stauffer, C. L., Becker, T., Reed, K. A., Ahn, M.-S., Arnold, N. P., et al. (2020). Clouds and convective self-aggregation in a multimodel ensemble of radiative-convective equilibrium simulations. *Journal of Advances in Modeling Earth Systems*, *12*(9), e2020MS002138. https://doi.org/10.1029/2020MS002138

Wyant, M. C., Bretherton, C. S., Bacmeister, J. T., Kiehl, J. T., Held, I. M., Zhao, M., et al. (2006). A comparison of low-latitude cloud properties and their response to climate change in three AGCMs sorted into regimes using mid-tropospheric vertical velocity. *Climate Dynamics*, *27*(2–3), 261–279. https://doi.org/10.1007/s00382-006-0138-4

Wyant, M. C., Khairoutdinov, M., & Bretherton, C. S. (2006). Climate sensitivity and cloud response of a GCM with a superparameterization. *Geophysical Research Letters*, *33*(6), L06714. https://doi.org/10.1029/2005GL025464

Zelinka, M. D., & Hartmann, D. L. (2010). Why is longwave cloud feedback positive? *Journal of Geophysical Research*, *115*(D16), D16117. https://doi.org/10.1029/2010JD013817

19422466, 2023, 5, Downloaded from https://agupubs.onlinelibrary.wiley.com/doi/10.1029/2022MS003516 by University Of St Andrews University, Wiley Online Library on [15/05/2023]. See the Terms and Conditions (https://onlinelibrary.wiley.com/terms-and-conditions) on Wiley Online Library for rules of use; OA articles are governed by the applicable Creative Commons License